Electronic Supplementary Information

Low temperature *in situ* Raman spectroscopy of electro-generated arylbis(arylthio)sulfonium ion

Kouichi Matsumoto,[a*] Yu Miyamoto,[a] Kazuaki Shimada,[a] Yusuke Morisawa,[a] Hendrik Zipse,[b] Seiji Suga,[c] Jun-ichi Yoshida,[d] Shigenori Kashimura,[a] and Tomonari Wakabayashi[a*]

[a] *Department of Chemistry, School of Science and Engineering, Kindai University, Kowakae 3-4-1, Higashi-Osaka, Osaka 577-8502, Japan*
[b] *Department of Chemistry, LMU München, Butenandtstrasse 5-13, D-81377 München, Germany*
[c] *Graduate School of Natural Science and Technology, Okayama University, Tsuhsima-Naka 3-1-1, Kita-ku, Okayama 700-8530, Japan*
[d] *Department of Synthetic Chemistry and Biological Chemistry, Graduate School of Engineering, Kyoto University, Nishikyo-ku, Kyoto 615-8510, Japan*

1. Materials.

Bu_4NBF_4 and trifluoromethanesulfonic acid (TfOH) were purchased from TCI. Dichloromethane was washed with water, distilled from P_2O_5, redistilled from dried K_2CO_3 to remove a trace amount of acid, and stored over molecular sieves 4A. ArSSAr (Ar = *p*-FC_6H_4) was prepared according to the procedure in the literature,[1] and identified by comparison of its spectral data with that of an authentic sample.[2] All the reactions were carried out under the dry N_2 atmosphere unless otherwise noted.

2. Experimental

2.1. Typical procedure.

Anodic oxidation of ArSSAr (Ar = *p*-FC_6H_4) was carried out in an H-type divided cell (4G glass filter) equipped with a carbon felt anode and a platinum plate cathode (40 mm x 20 mm). In the anodic chamber was placed a solution of Bu_4NBF_4 (791 mg, 2.40 mmol) in CH_2Cl_2 (10.0 mL) and ArSSAr (Ar = *p*-FC_6H_4, 318 mg, 1.25 mmol). In the cathodic chamber were placed the same solution, Bu_4NBF_4 (793 mg, 2.41 mmol)/CH_2Cl_2 (10.0 mL), and trifluoromethanesulfonic acid (TfOH) (74 μL, c.a. 126 mg, c.a. 0.840 mmol) for the effective reduction in the chathodic chamber. The constant electrolysis current (8.0 mA) was conducted to accumulate $ArS(ArSSAr)^+$ in the solution at 195 K using a magnetic stirrer. The electrolyzed solution was subjected to spectroscopic monitoring. The electrochemical cell was kept at 195 K throughout the experiment by bathing it into a coolant mixture of dry-ice/acetone.

As the electrochemical reaction proceeds, the solution in the anodic camber turned from a yellow transparent solution into a dark brownish solution, because accumulated cations might be oxidized further into unknown by-products. To minimize the loss of transparency for both the excitation laser beam and Raman scattering light signals, we chose the excitation at a relatively long wavelength of 785 nm.

2.2. Raman spectroscopy

A laser beam from a fiber-coupled output of cw laser, Toptica XTRA, 250 mW at 785 nm, was conducted through the solution in the anodic chamber of the electrochemical cell. Scattered light was collected in the direction perpendicular to the axis of the laser beam by using a combination of quartz lenses focusing the light on the surface of the entrance cross section of the bundle of forty optical fibers with a 100 μm diameter for each. The optical components were contained in a vacuum-tight glass tube sealed with rubber *o*-rings and partly dipped into the reactant solution. The electrochemical cell was independently purged with N_2

gas to avoid humidity in air. For the measurement, the vacuum seal of the optical component was crucial in avoiding frost, which scatters both the excitation and signal lights.

The collected light was conducted through the optical fibers to a spectrometer for dispersion, Acton 320 PI (1200 G/mm blazed at 500 nm or 600 G/mm blazed at 1000 nm), and detected by using a liquid-nitrogen cooled CCD array detector, PyLoN:256-OE 1024 x 256 pixels of 26 x 26 μm^2. To minimize stray light, a sharp-edge long-pass filter, Semrock RazorEdge 785R (o.d. $<10^{-6}$ at 785 nm), was placed in front of the entrance slit of the spectrometer, where the image of the exit cross section of the fiber bundle with vertically aligned forty optical fibers was focused. Spectra were accumulated for 6 min 40 sec (a 4-sec exposure time by 100 times accumulation) for each and redundantly stored one by one for 4 hours (400 sec by 60 spectra) during the electrolysis. Spectral resolution was ~0.2 nm, which corresponds to ~3 cm^{-1} at 815 nm where a Raman band of 470 cm^{-1} was observed.

In Fig. S1, Raman spectra of precursory materials at ambient temperature are compared to associate the observed bands with their carriers, i.e., the precursor, ArSSAr (Ar = *p*-FC_6H_4), the electrolyte, Bu_4NBF_4, and the solvent, CH_2Cl_2. Trace a depicts all the Raman bands of ArSSAr. Trace d represents the bands of the solvent, CH_2Cl_2. In the solution of these two reagents, namely trace c, all the Raman spectral features are seen simply as a superposition of the individual spectra, indicating negligible interaction between ArSSAr and CH_2Cl_2. When the electrolyte is added, the situation is not very much changed, though a lot of bands due to ions from the electrolyte, namely NBu_4^+ and BF_4^-, are superposed.

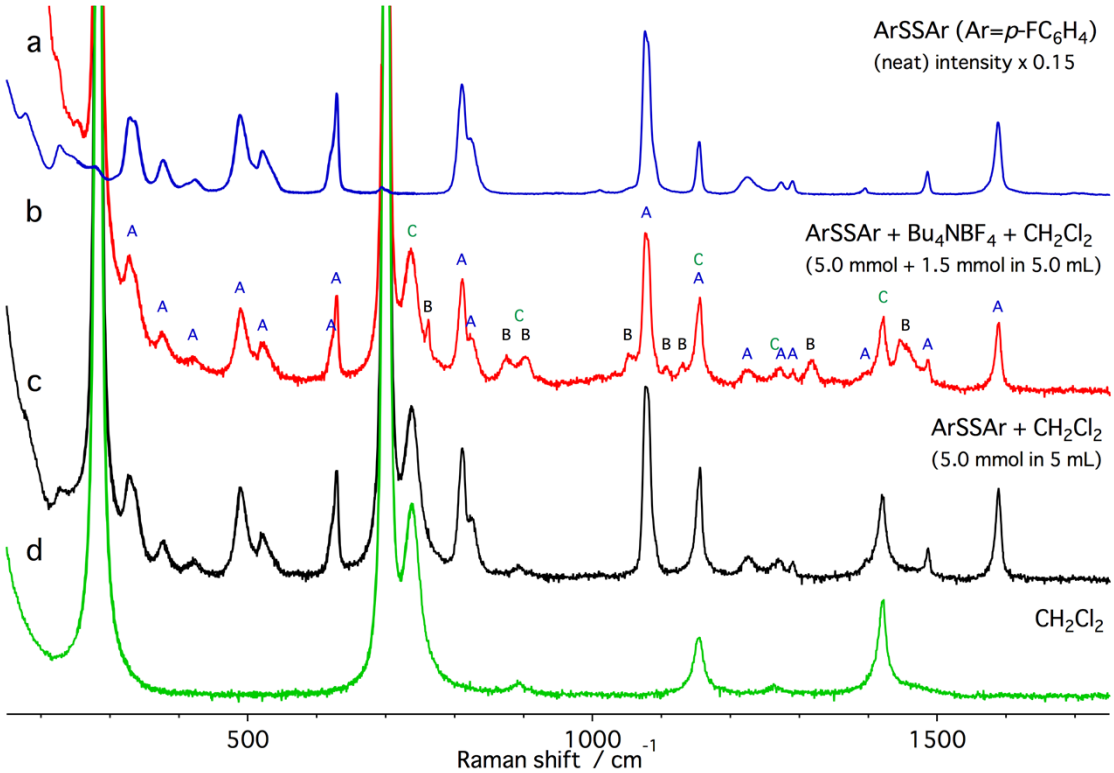

Fig. S1. Raman spectra at ambient temperature of materials used in the present work. In Trace b for the mixture, Raman bands annotated with A belong to ArSSAr (Ar = *p*-FC_6H_4), bands with B belong to the ions from Bu_4NBF_4, and bands with C belong to CH_2Cl_2.

Note here that, in the spectral region at 300-700 cm^{-1} in-between the two strong bands of the solvent, only a series of bands due to precursory ArSSAr molecules as annotated with A are discernible. This is an advantage for the study of spectral changes from the reactant molecules to the product molecular cations.

2.3. Molecular orbital calculations

Gaussian 09, revision C.01, quantum chemical package[3] was used for molecular orbital calculations of Raman spectra for chemical species of interest, including the precursory ArSSAr (Ar = *p*-FC_6H_4), the target arylbis(arylthio)sulfonium ion, $ArS(ArSSAr)^+$, and monomeric neutral radical, ArS, for considerations on the spectral assignment. Using the tightly optimized geometry, Raman frequencies as well as their intensities were calculated at the B3LYP/6-311++G(2d,p) level of theory. For the monomer radical, ArS, UB3LYP/6-311++G(2d,p) was adopted for its spin-doublet ground state. The optimized geometries are illustrated in Fig. S2.

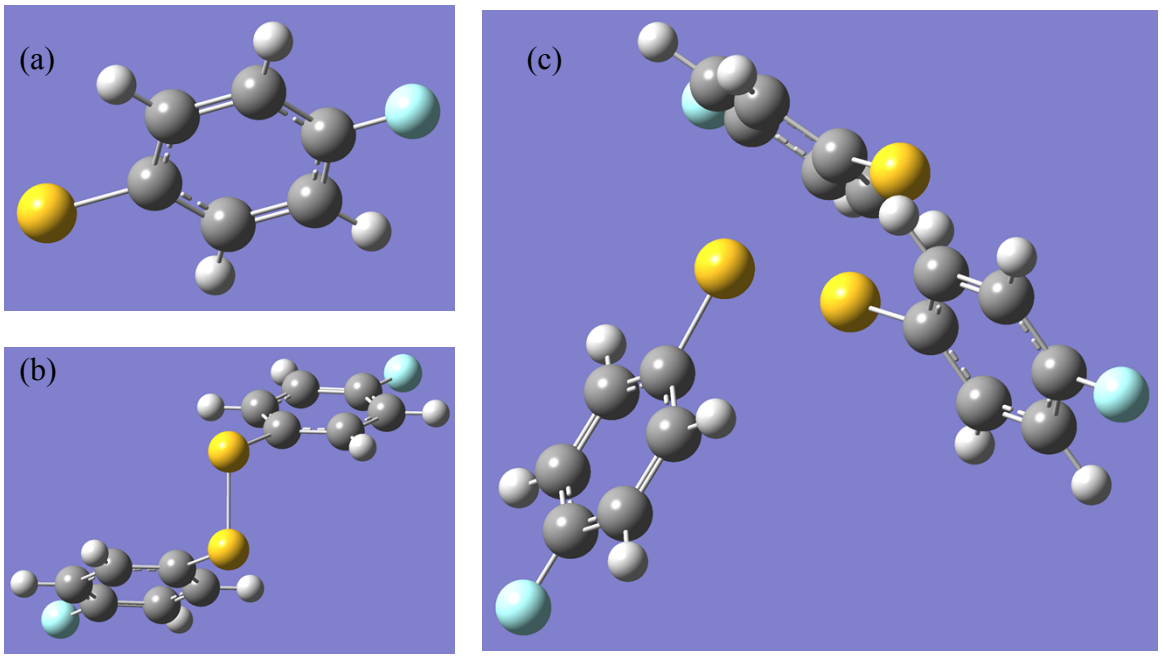

Fig. S2. Geometry-optimized structures for (a) monomer radical, ArS (Ar = *p*-FC_6H_4) (*doublet*), (b) disulfide, ArSSAr (*singlet*), and (c) trimer cation, $ArS(ArSSAr)^+$ (*singlet*).

Vibrational modes thus obtained are listed in Tables T1-T3, namely for monomer radical ArS (T1), disulfide ArSSAr (T2), and trimer cation $ArS(ArSSAr)^+$ (T3). In Table T1, among all the $3N$- 6 = 30 vibrational modes in ArS, 26 modes are typified as a-z from low frequencies except for four C-H stretching modes having distinctly high frequencies. In Table T2 for disulfides, ArSSAr, the same type of vibrational modes, namely a-z, appears twice in the close vicinity to each other, as a quasi-degenerate couple of the same intra-monomeric vibrational mode with basically the same frequency but coupled differently in a symmetric phase or in an anti-symmetric phase. The total degrees of freedom for nuclear motions increase twice from $3N$ = 36 for ArS to $3N$ = 72 for ArSSAr. Since a total of 6 degrees of freedom are reserved for the translational and rotational degrees of freedom for the molecular center of mass, the difference in the total vibrational degrees of freedom, i.e., 66 (ArSSAr) – 30 (ArS) × 2 = 6, remains as the number of new vibrational modes in ArSSAr, which are converted from the intermolecular motions between the two parts, ArS and SAr. In a weakly bound molecular complex, these intermolecular vibrations have low frequencies, typically <100 cm^{-1}. When a covalent bond of S-S is formed in-between, one of the intermolecular vibranal frequencies comes to a higher frequency region in 300-500 cm^{-1}. These additional intermolecular vibrational modes in ArSSAr are indicated in a background colour in red without noting any type a-z in Table T2. Among others, this S-S stretching mode at 451 cm^{-1} can exhibit a conspicuous Raman activity.

In the same manner, upon shifting from dimer to trimer, in addition to the 26 three-fold degenerate bands of modes, a-z, a total 12 inter-molecular vibrational modes are discernible at low frequency regions for ArS(ArSSAr)$^+$ in Table T3. Among the total 102 vibrational modes in ArS(ArSSAr)$^+$, 32 modes show vibrational frequencies in 300-850 cm^{-1} and two thirds of them represent Raman activities. Since most of these modes are triply degenerate and since part of them cannot be strongly Raman active, only several bands remain for necessary considerations for the carrier of the observed Raman bands. Two S-S stretching modes in the bent S_3 moiety, namely symmetric and anti-symmetric, constitute the most important Raman bands, which are predicted at 458 cm^{-1} and 434 cm^{-1}, respectively (see Table T3). Dragged and/or repelled by motions of the ring deformation in the three *p*-FC_6H_4 groups, sulfur atoms in the central S_3 unit can have large displacements to enhance its Raman activity. Such modes are also important for the assignment of the Raman spectra, as exemplified in the intrinsically degenerate three modes at 378, 364, and 363 cm^{-1}, namely type d (see Table T3). Judging from its remarkable intensity and relative positions over several bands, the observed band I at 427 cm^{-1} is plausibly attributed to such a mode of vibration. One of the other out-of-plane ring-deformation modes can couple to represent a substantial Raman activity as predicted at 298 cm^{-1} as one of the type c modes (see Table T3).

Fig. S3 compares calculated Raman spectra for monomer radical, ArS, disulfide, ArSSAr, and trimer cation, ArS(ArSSAr)$^+$. The two-fold and three-fold degeneracies are seen by peak positions, a-z, in the dimer and trimer, respectively. The peaks of the same type are superposed constituting a band of peaks. This degeneracy due to independent vibrations in each of the three *p*-FC_6H_4-S groups is remarkable for higher frequency vibrational modes, >500 cm^{-1}. For lower frequency vibrational modes in <500 cm^{-1}, reflecting the nature of delocalized large amplitude motions in such a low-symmetry structures of C_1 point group symmetry for ArS(ArSSAr)$^+$, the degeneracy is lifted and easily couple with the vibrations of S-S-S bonds to show a conspicuous enhancements of a group of Raman bands in 295-470 cm^{-1} (red triangles).

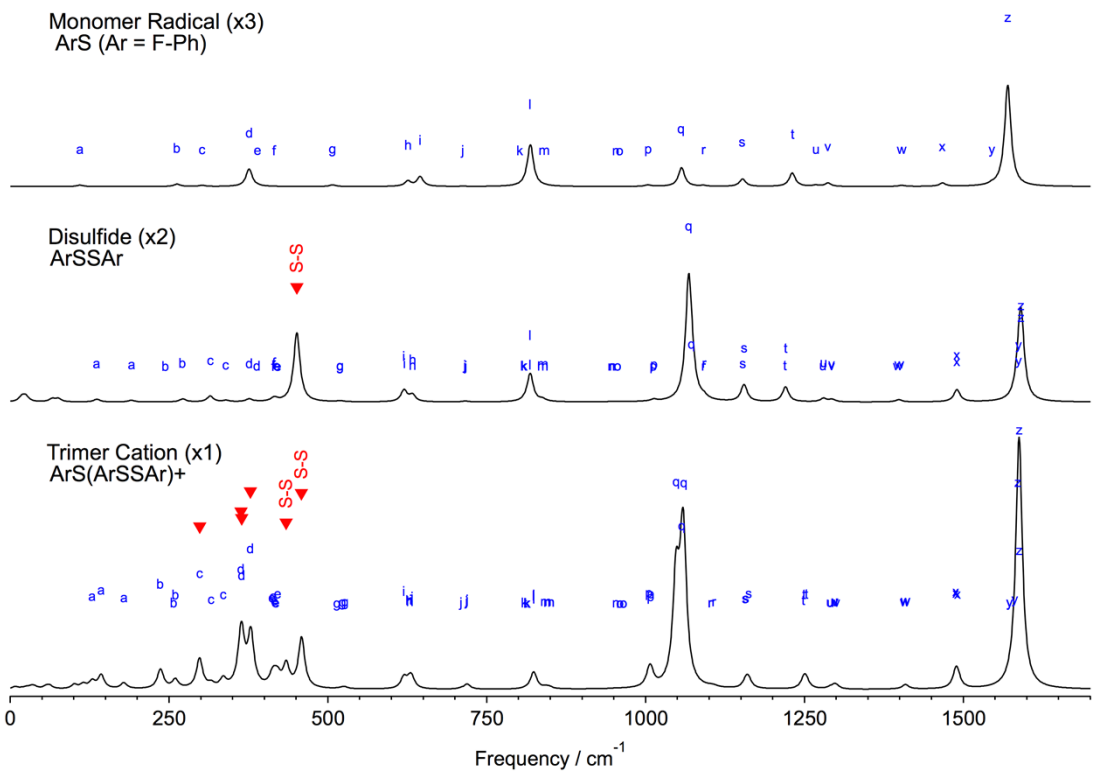

Fig. S3. Comparison of calculated Raman spectra for monomer radical, ArS, disulfide, ArSSAr, and trimer cation, ArS(ArSSAr)$^+$, at UB3LYP/ or B3LYP/6-311++G(2d,p). Each

Raman mode signal is drawn by a line width of 6 cm^{-1}.

References

1 M. Hirano, S. Yakabe, H. Monobe and T. Morimoto, *J. Chem. Research (S)*, 1998, 472.

2 D. P. Becker, C. I. Villamil, T. E. Barta, L. J. Bedell, T. L. Boehm, G. A. DeCrescenzo, J. N. Freskos, D. P. Getman, S. Hockerman, R. Heintz, S. C. Howard, M. H. Li, J. J. McDonald, C. P. Carron, C. L. Funckes-Shippy, P. P. Mehta, G. E. Munie and C. A. Swearingen, *J. Med. Chem.*, 2005, **48**, 6713.

3 Gaussian 09, Revision C.01, M. J. Frisch, G. W. Trucks, H. B. Schlegel, G. E. Scuseria, M. A. Robb, J. R. Cheeseman, G. Scalmani, V. Barone, B. Mennucci, G. A. Petersson, H. Nakatsuji, M. Caricato, X. Li, H. P. Hratchian, A. F. Izmaylov, J. Bloino, G. Zheng, J. L. Sonnenberg, M. Hada, M. Ehara, K. Toyota, R. Fukuda, J. Hasegawa, M. Ishida, T. Nakajima, Y. Honda, O. Kitao, H. Nakai, T. Vreven, J. A. Montgomery, Jr., J. E. Peralta, F. Ogliaro, M. Bearpark, J. J. Heyd, E. Brothers, K. N. Kudin, V. N. Staroverov, T. Keith, R. Kobayashi, J. Normand, K. Raghavachari, A. Rendell, J. C. Burant, S. S. Iyengar, J. Tomasi, M. Cossi, N. Rega, J. M. Millam, M. Klene, J. E. Knox, J. B. Cross, V. Bakken, C. Adamo, J. Jaramillo, R. Gomperts, R. E. Stratmann, O. Yazyev, A. J. Austin, R. Cammi, C. Pomelli, J. W. Ochterski, R. L. Martin, K. Morokuma, V. G. Zakrzewski, G. A. Voth, P. Salvador, J. J. Dannenberg, S. Dapprich, A. D. Daniels, O. Farkas, J. B. Foresman, J. V. Ortiz, J. Cioslowski and D. J. Fox, Gaussian, Inc., Wallingford CT, 2010.

Table T1.

ArS (Ar = *p*-FC_6H_4) Monomer Radical [neutral, doublet] at UB3LYP/6-311++G(2d,p).

Mode	Frequency	IR Intensity	Raman Activity	Scaled Freq.	Assign			activity	type
No.	cm^{-1}	10^{-40} $esu^2\ cm^2$	$Å^2$/AMU	x0.98	bond/group	motion	direction		
1	111.8	2.0	1.2	110	S-CCCC-F	single bend	out-of-plane		a
2	267.7	1.3	2.2	262	C-C-S	head-waving skew	in-plane		b
3	308.1	0.5	1.0	302	S-CCCC-F	dolphin kick	out-of-plane		c
4	383.4	5.7	16.4	376	S-CCCC-F	ring squaring	in-plane	IR/Raman	d
5	397.4	0.0	0.2	389	C-C-C	skew	out-of-plane		e
6	423.2	3.4	0.0	415	C-C-F	tail-waving skew	in-plane		f
7	517.7	15.5	1.5	507	C-C-C	butterfly	out-of-plane	IR	g
8	638.4	0.0	5.3	626	C-C-C	ring squeeze	in-plane	Raman	h
9	658.0	12.9	9.6	645	C-S	stretch	in-plane	IR/Raman	i
10	727.0	0.0	0.2	712	C-C-C	ring chairing	out-of-plane		j
11	818.0	0.0	0.0	802	C-C-H	paddling	out-of-plane		k
12	835.1	13.7	42.9	818	C-S/C-F	ring squaring	in-plane	IR/Raman	l
13	856.7	62.2	0.2	840	C-C-H	zigzag bend	out-of-plane	IR	m
14	972.3	0.0	0.0	953	C-C-H	butterflying	out-of-plane		n
15	978.5	0.0	0.0	959	C-C-H	crawling	out-of-plane		o
16	1024.0	2.0	1.6	1004	C-C	ring triangularing	in-plane		p
17	1077.9	32.0	20.4	1056	C-C/C-S	stretch/ring breathing	in-plane	IR/Raman	q
18	1112.8	4.0	0.9	1091	C-C	anti-sym ring defoem	in-plane		r
19	1175.9	40.3	8.2	1152	C-C	sym-ring defoem	in-plane	IR/Raman	s
20	1255.7	153.4	15.2	1231	S-F	stretch	in-plane	IR/Raman	t
21	1293.7	0.1	1.4	1268	C-C/C-S	2-fold ring twist	in-plane		u
22	1313.1	7.3	3.8	1287	C-C/C-F	1-fold ring twist	in-plane	IR	v
23	1431.5	7.1	1.3	1403	C-C	ring defoem	in-plane	IR	w
24	1496.9	45.4	3.9	1467	C-C/C-F/C-S	ring defoem	in-plane	IR	x
25	1576.1	7.8	1.4	1545	C-C	2-fold ring twist	in-plane	IR	y
26	1601.8	213.9	123.8	1570	C-C/C-F	ring squaring	in-plane	IR/Raman	z
27	3190.4	1.1	20.2	3127	C-H	stretch	in-plane	Raman	
28	3191.3	0.1	97.9	3127	C-H	stretch	in-plane	Raman	
29	3202.9	0.5	14.0	3139	C-H	stretch	in-plane	Raman	
30	3204.7	2.4	250.7	3141	C-H	sym-stretch breathing	in-plane	Raman	

*Colours distinguish prominent Raman modes (yellow) or in-plane (green) or out-of-plane (orange) vibrational modes.

*Type depicts each of the 26 vibrational modes other than four C-H stretching modes as a-z from low frequencies.

ArSSAr (Ar = *p*-FC_6H_4) Disulfide [neutral, singlet] at B3LYP/6-311++G(2d,p).

Mode	Frequency	IR Intensity	Raman Activity	Scaled Freq.	Assign				activity	type
No.	cm^{-1}	10^{-40} $esu^2\ cm^2$	$Å^2$/AMU	x0.98	bond/group	motion	direction	phase		
1	17.9	0.0	5.1	18	S-S	rotation Z	inter molecular ring overlap		Raman	
2	22.1	0.1	3.0	22	C-S	rotation anti-sym	inter molecular dihedral angle			
3	25.3	0.0	5.3	25	C-S	rotation sym	inter molecular dihedral angle		Raman	
4	67.2	0.3	3.9	66	S-S	rotation X	inter molecular			
5	76.8	0.2	4.1	75	S-S	rotation Y	inter molecular			
6	138.9	0.1	3.7	136	S-CCCC-F	single bend	out-of-plane	sym		a
7	194.4	1.2	2.3	191	S-CCCC-F			anti-sym		a
8	249.2	1.5	0.0	244	C-C-S	head-waiving skew	in-plane	anti-sym		b
9	277.0	1.5	4.1	271	C-C-S			sym		b
10	321.0	0.4	8.1	315	S-CCCC-F/S-S	dolphin kick	out-of-plane	sym	Raman	c
11	346.4	10.0	1.9	339	S-CCCC-F/S-S			anti-sym	IR	c
12	383.5	10.1	3.9	376	S-CCCC-F/S-S	ring squaring	in-plane	sym	IR	d
13	395.6	8.3	0.2	388	S-CCCC-F/S-S		/out-of-plane	anti-sym	IR	d
14	421.2	3.5	0.0	413	C-C-C	tail-waving skew	in-plane	anti-sym		f
15	423.2	0.5	4.5	415	C-C-C			sym		f
16	427.5	0.1	1.0	419	C-C-C	skew	out-of-plane	sym		e
17	429.3	0.2	0.0	421	C-C-C			anti-sym		e
18	460.1	3.0	100.0	451	S-S	stretch	inter molecular	sym	Raman	
19	529.5	8.0	0.9	519	C-C-C	butterfly	out-of-plane	sym	IR	g
20	529.5	32.7	0.5	519	C-C-C			anti-sym	IR	g
21	632.0	4.3	13.8	619	C-S	stretch	in-plane	sym	Raman	i
22	633.1	11.2	3.7	620	C-S			anti-sym	IR	i
23	645.6	0.1	1.3	633	C-C-C	ring squeeze	in-plane	anti-sym		h
24	645.8	0.0	8.8	633	C-C-C			sym	Raman	h
25	730.1	0.4	1.1	715	C-C-C	ring chairing	out-of-plane	sym		j
26	732.1	0.2	0.3	717	C-C-C			anti-sym		j
27	824.6	0.1	0.2	808	C-C-H	paddling	out-of-plane	anti-sym		k
28	825.6	1.0	0.5	809	C-C-H			sym		k
29	834.8	21.1	42.8	818	C-S/C-F	ring-squaring	in-plane	sym	IR/Raman	l
30	835.1	14.5	1.8	818	C-S/C-F			anti-sym	IR	l
31	854.9	6.3	3.2	838	C-C-H	zigzag bend	out-of-plane	sym	IR	m
32	855.3	93.5	0.2	838	C-C-H			anti-sym	IR	m
33	964.9	0.2	0.2	946	C-C-H	butterflying	out-of-plane	sym		n
34	967.2	0.1	0.1	948	C-C-H			anti-sym		n
35	975.1	0.2	0.1	956	C-C-H	crawling	out-of-plane	anti-sym		o
36	975.3	0.1	0.4	956	C-C-H			sym		o
37	1033.1	6.9	0.2	1012	C-C	ring triangularing	in-plane	anti-sym	IR	p
38	1033.4	2.3	2.7	1013	C-C			sym		p
39	1089.4	1.8	195.2	1068	C-C/C-S	stretch/ring breathing	in-plane	sym	Raman	q
40	1094.4	2.4	30.9	1072	C-C/C-S			anti-sym	Raman	q
41	1113.6	6.7	0.2	1091	C-C	anti-sym ring deform	in-plane	anti-sym	IR	r
42	1114.1	3.9	4.1	1092	C-C			sym		r
43	1176.5	62.3	3.6	1153	C-C	sym-ring deform	in-plane	anti-sym	IR	s
44	1178.6	21.7	25.4	1155	C-C			sym	IR/Raman	s
45	1244.0	168.9	0.6	1219	C-F	stretch	in-plane	anti-sym	IR	t
46	1244.9	136.2	24.8	1220	C-F			sym	IR/Raman	t
47	1305.6	0.6	0.9	1279	C-C/C-S	2-fold ring twist	in-plane	anti-sym		u
48	1306.0	0.0	5.0	1280	C-C/C-S			sym	Raman	u
49	1319.5	6.9	0.7	1293	C-C/C-F	1-fold ring twist	in-plane	anti-sym	IR	v
50	1319.7	2.6	3.4	1293	C-C/C-F			sym		v
51	1425.8	4.5	0.9	1397	C-C	ring deform	in-plane	anti-sym		w
52	1427.1	1.6	3.1	1399	C-C			sym		w
53	1520.0	72.0	15.7	1490	C-C/C-F/C-S	ring deform	in-plane	sym	IR/Raman	x
54	1520.6	95.4	6.7	1490	C-C/C-F/C-S			anti-sym	IR	x
55	1618.9	2.9	8.1	1587	C-C	2-fold ring twist	in-plane	anti-sym	Raman	y
56	1619.1	21.9	30.0	1587	C-C			sym	IR/Raman	y
57	1623.1	53.2	84.4	1591	C-S/C-F	ring squaring	in-plane	sym	IR/Raman	z
58	1623.5	84.5	68.0	1591	C-S/C-F			anti-sym	IR/Raman	z
59	3186.6	1.7	31.2	3123	C-H	stretch	in-plane	sym	Raman	
60	3186.7	1.3	12.4	3123	C-H	stretch	in-plane	anti-sym	Raman	
61	3187.8	1.6	19.7	3124	C-H	stretch	in-plane	anti-sym	Raman	
62	3187.9	0.0	106.3	3124	C-H	stretch	in-plane	sym	Raman	
63	3200.2	2.4	9.7	3136	C-H	stretch	in-plane	anti-sym	Raman	
64	3200.3	0.3	118.7	3136	C-H	sym-stretch breathing	in-plane	sym	Raman	
65	3201.5	3.5	68.1	3138	C-H	stretch	in-plane	anti-sym	Raman	
66	3201.6	1.7	394.7	3138	C-H	sym-stretch breathing	in-plane	sym	Raman	

*Colours distinguish prominent Raman modes (yellow) or in-plane (green) or out-of-plane (orange) vibrational modes.

*On colours in red are the intermolecular vibrational modes including an S-S stretching mode, all associated with the dimer.

*Phase denotes the distinction of the relative motion in the two ArS moieties in the disulfide ArSSAr.

*Type depicts each of the 26 vibrational modes of a-z from low frequencies as deffined for the monomer radical ArS.

*Each type in the a-z modes is doubly degenerated in the disulfide ArSSAr.

Table T2.

$ArS(ArSSAr)^+$ (Ar = p-FC_6H_4) Trimer Cation [mono-cation, singlet] at B3LYP/6-311++G(2d,p).

Mode	Frequency	IR Intensity	Raman Activity	Scaled Freq.	Assign				activity	type
No.	cm^{-1}	10^{-40} $esu^2\ cm^2$	$Å^2$/AMU	x0.98	bond/group	motion	direction	phase		
1	7.4	0.1	6.1	7		inter molecular	libration	S_3 translation	Raman	
2	17.7	0.1	1.6	17		inter molecular	libration	S_3 translation	Raman	
3	25.3	0.3	3.9	25		inter molecular	libration	S_3 translation		
4	33.1	0.2	9.0	32	C-S	rotation	all		Raman	
5	36.8	0.1	2.4	36	C-S	rotation	center			
6	39.0	0.2	3.8	38	C-S	rotation	sides			
7	57.7	0.2	9.9	57		inter molecular	swing	S_3 rotation	Raman	
8	63.2	0.0	7.5	62		inter molecular	swing	S_3 rotation	Raman	
9	102.7	1.2	11.0	101		inter molecular	swing	S_3 bend	Raman	
10	117.0	0.3	12.2	115		inter molecular	swing	S_3 bend	Raman	
11	131.4	0.5	19.5	129	S-CCCC-F			centre-side1	Raman	a
12	145.8	0.2	36.8	143	S-CCCC-F	single bend	out-of-plane	centre-side2	Raman	a
13	182.2	0.6	16.0	179	S-CCCC-F			all	Raman	a
14	241.1	4.5	53.5	236	C-C-S			centre	Raman	b
15	262.0	2.8	1.0	257	C-C-S	head-waiving skew	in-plane	side2		b
16	265.0	0.5	23.2	260	C-C-S			side1	Raman	b
17	303.8	1.9	83.3	298	S-CCCC-F/S-S			S_3 anti-sym str	Raman	c
18	322.4	1.4	10.5	316	S-CCCC-F/S-S	dolphin kick	out-of-plane	S_3 bend	Raman	c
19	341.8	20.8	24.4	335	S-CCCC-F/S-S			S_3 translation	IR/Raman	c
20	370.2	59.2	95.2	363	S-CCCC-F/S-S		in-plane	side2/S_3 anti-sym str	IR/Raman	d
21	371.9	17.9	77.4	364	S-CCCC-F/S-S	ring squaring	/out-of-plane	side1/S_3 anti-sym str	IR/Raman	d
22	386.1	6.6	151.5	378	S-CCCC-F/S-S			centre/S_3 anti-sym str	IR/Raman	d
23	419.9	1.4	15.9	412	C-C-C			centre out-of-plane	Raman	e,f
24	422.4	0.7	19.9	414	C-C-C			center in-plane/all	Raman	e,f
25	424.7	0.1	6.5	416	C-C-C	tail-waving skew	in-plane	side2 out-of-plane	Raman	e,f
26	425.9	3.3	2.3	417	C-C-C	/skew	/out-of-plane	side1 in-plane		e,f
27	426.7	2.6	0.8	418	C-C-C			side2 in-plane		e,f
28	429.4	2.1	26.7	421	C-C-C			side1 out-of-plane	Raman	e,f
29	443.0	13.1	64.6	434	S-S	stretch	inter molecular	S_3 anti-sym str	IR/Raman	
30	467.7	1.3	146.3	458	S-S			S_3 sym str (breathing)	Raman	
31	524.5	31.6	0.4	514	C-C-C			centre	IR	g
32	533.4	11.4	3.2	523	C-C-C	butterfly	out-of-plane	side1	IR	g
33	537.5	8.6	3.6	527	C-C-C			side2	IR	g
34	631.9	1.7	33.4	619	C-S	stretch	in-plane	centre	Raman	
35	640.5	0.7	7.5	628	C-C-C			centre	Raman	h
36	641.8	0.3	4.8	629	C-C-C	ring squeeze	in-plane	side2		h
37	642.0	0.3	5.4	629	C-C-C			side1	Raman	h
38	643.3	2.7	10.1	630	C-S	stretch	in-plane	side1	Raman	i
39	645.2	1.9	17.6	632	C-S			side2	Raman	i
40	723.2	0.3	2.3	709	C-C-C			center		j
41	732.8	1.2	6.3	718	C-C-C	ring chairing	out-of-plane	side1	Raman	j
42	734.2	1.6	9.5	719	C-C-C			side2	Raman	j
43	825.3	0.1	0.9	809	C-C-H			centre		k
44	829.9	0.2	0.1	813	C-C-H	paddling	out-of-plane	side2		k
45	830.5	0.1	0.1	814	C-C-H			side1		k
46	839.3	7.9	20.5	823	C-S/C-F			center	IR/Raman	l
47	841.1	14.3	23.2	824	C-S/C-F	ring-squaring	in-plane	side1	IR/Raman	l
48	841.3	9.5	11.5	824	C-S/C-F			side2	IR/Raman	l
49	859.8	46.9	5.0	843	C-C-H			centre	IR/Raman	m
50	865.5	57.3	2.6	848	C-C-H	zigzag bend	out-of-plane	side2	IR	m
51	865.8	46.3	2.6	848	C-C-H			side1	IR	m
52	972.9	2.3	0.7	953	C-C-H			centre		n
53	979.1	0.2	0.0	960	C-C-H	butterflying	out-of-plane	side2		n
54	979.7	0.6	0.0	960	C-C-H			side1		n
55	979.7	0.2	0.2	960	C-C-H			centre		o
56	984.7	0.1	0.1	965	C-C-H	crawling	out-of-plane	side2		o
57	984.9	0.1	0.0	965	C-C-H			side1		o
58	1025.7	1.3	28.7	1005	C-C			centre	Raman	p
59	1028.3	0.5	18.7	1008	C-C	ring triangularing	in-plane	side2	Raman	p
60	1028.4	0.2	26.1	1008	C-C			side1	Raman	p
61	1069.0	34.0	338.9	1048	C-C/C-S			centre	IR/Raman	q
62	1078.8	96.7	216.1	1057	C-C/C-S	stretch/ring breathing	in-plane	anti-sym sedes	IR/Raman	q
63	1081.4	75.9	336.0	1060	C-C/C-S			sym sides	IR/Raman	q
64	1123.2	3.4	1.1	1101	C-C			side1		r
65	1123.9	4.3	1.4	1101	C-C	anti-sym ring deform	in-plane	side2		r
66	1130.1	5.9	3.8	1107	C-C			center	IR	r
67	1181.0	88.8	12.8	1157	C-C			anti-sym sides	IR/Raman	s
68	1182.1	127.2	13.3	1158	C-C	sym-ring deform	in-plane	sym sides	IR/Raman	s
69	1185.4	11.4	26.8	1162	C-C			sym all	Raman	s
70	1273.9	225.7	8.0	1248	C-F			anti-sym sides	IR/Raman	t
71	1274.7	292.6	24.6	1249	C-F	stretch	in-plane	sym sides	IR/Raman	t
72	1278.1	118.8	24.9	1253	C-F			centre	IR/Raman	t
73	1315.9	0.2	2.8	1290	C-C/C-S			side1		u
74	1316.9	0.0	2.5	1291	C-C/C-S	2-fold ring twist	in-plane	side2		u
75	1323.6	7.9	5.8	1297	C-C/C-S			side1+centre	IR/Raman	u
76	1324.3	8.7	6.4	1298	C-C/C-F			side2	IR/Raman	v
77	1324.9	0.9	4.0	1298	C-C/C-F	1-fold ring twist	in-plane	all		v
78	1327.7	8.0	3.4	1301	C-C/C-F			centre	IR	v
79	1436.8	8.0	3.8	1408	C-C			side1	IR	w
80	1437.0	8.4	5.3	1408	C-C	ring deform	in-plane	side2	IR/Raman	w
81	1438.2	7.6	7.4	1409	C-C			centre	IR/Raman	w
82	1518.3	54.7	28.5	1488	C-C/C-F/C-S			anti-sym sides	IR/Raman	x
83	1518.8	58.9	32.9	1488	C-C/C-F/C-S	ring deform	in-plane	sym sides	IR/Raman	x
84	1521.8	84.3	25.3	1491	C-C/C-F/C-S			centre	IR/Raman	x
85	1605.2	5.1	2.7	1573	C-C			anti-sym sides	IR	y
86	1605.5	6.9	1.9	1573	C-C	2-fold ring twist	in-plane	sym sides	IR	y
87	1613.1	18.5	12.2	1581	C-C			centre	IR/Raman	y
88	1618.9	314.9	336.5	1586	C-S/C-F			anti-sym sides	IR/Raman	z
89	1620.0	338.3	146.8	1588	C-S/C-F	ring squaring	in-plane	centre	IR/Raman	z
90	1620.8	35.0	482.3	1588	C-S/C-F			sym all	IR/Raman	z
91	3189.2	0.2	24.9	3125	C-H	stretch	in-plane	centre	Raman	
92	3193.6	0.2	32.4	3130	C-H	stretch	in-plane	side2	Raman	
93	3194.0	0.2	21.8	3130	C-H	stretch	in-plane	side1	Raman	
94	3194.8	0.2	16.3	3131	C-H	stretch	in-plane	centre	Raman	
95	3194.9	0.4	55.0	3131	C-H	stretch	in-plane	side1	Raman	
96	3196.8	0.2	45.9	3133	C-H	stretch	in-plane	side2	Raman	
97	3207.7	2.0	69.4	3144	C-H	stretch	in-plane	side1	Raman	
98	3207.8	2.4	105.7	3144	C-H	stretch	in-plane	side2	Raman	
99	3208.5	4.0	192.3	3144	C-H	stretch	in-plane	centre	Raman	
100	3208.5	0.6	155.2	3144	C-H	stretch	in-plane	side1	Raman	
101	3209.0	0.7	172.9	3145	C-H	stretch	in-plane	side2	Raman	
102	3209.1	1.2	259.8	3145	C-H	stretch	in-plane	centre	Raman	

*Colours distinguish prominent Raman modes (yellow) or in-plane (green) or out-of-plane (orange) vibrational modes.

*On colours in red are the intermolecular vibrational modes including S_3-oriented modes, all associated with the trimer cation.

*On colours in purple or gray are the coupled modes between S_3 modes and phenyl-ring deformation modes, some of which have substantial Raman activities.

*Phase denotes the distinction of the ArS moiety(ies) having major displacements in the trimer cation $ArS(ArSSAr)^+$.

*Types depict each of the 26 vibrational modes of a-z from low frequencies as deffined for the monomer radical ArS.

*Each type in the a-z modes is triply degenerated in the trimer cation $ArS(ArSSAr)^+$.

Table T3.